

Non-linear screening effects in high energy hadronic interactions

S. Ostapchenko*

Forschungszentrum Karlsruhe, Institut für Kernphysik, 76021 Karlsruhe, Germany

D. V. Skobeltsyn Institute of Nuclear Physics, Moscow State University, 119992 Moscow, Russia

24th May 2019

Abstract

Non-linear effects in hadronic interactions are treated by means of enhanced Pomeron diagrams. The basic assumption of the scheme is that Pomeron-Pomeron interaction vertex is dominated by soft partonic processes. It is shown that the approach allows to resolve a seeming inconsistency between realistic parton momentum distributions, measured in deep inelastic scattering experiments, and the energy behavior of total proton-proton cross section. An important feature of the proposed scheme is that the contribution of semi-hard processes to the interaction eikonal contains a significant non-factorizable part. On the other hand, the approach preserves the QCD factorization picture for inclusive high- p_t jet production.

1 Introduction

It had been realized long ago that non-linear effects are inevitably present in high energy hadronic interactions [1, 2, 3]. In particular, the need for such corrections appears quite evident when considering small x behavior of parton momentum distribution functions (PDFs) at some finite virtuality scale Q^2 : due to a fast increase of, e.g., gluon PDF $G(x, Q^2)$ in the $x \rightarrow 0$ limit parton density in a restricted volume may reach arbitrarily large values [3]. As an indirect manifestation of the problem one may consider too fast, compared to measurements, energy increase of total proton-proton cross section, when calculated using the “QCD-eikonal” scheme [4],

if realistic PDFs are employed. A possible solution of the puzzle could be provided by the GLR approach [3], which introduces non-linear corrections to perturbative QCD evolution. The formalism implies that parton density is saturated at some x -dependent virtuality scale $Q_{\text{sat}}^2(x)$; dynamical parton evolution is then only possible in the region of sufficiently high virtualities $|q|^2 > Q_{\text{sat}}^2(x)$. However, the saturation picture is inapplicable for peripheral hadronic collisions dominated by non-perturbative “soft” processes.

In this paper a phenomenological treatment of non-linear screening corrections is presented, based on the assumption that corresponding effects are of non-perturbative origin [5]. Total proton-proton cross section and proton structure function (SF) F_2 are calculated in the framework of Gribov’s Reggeon scheme [1], using a phenomenological soft Pomeron description for low virtuality parton cascades and employing the “semi-hard Pomeron” formalism [6, 7] to treat cascades which at least partly develop in the region of comparatively large virtualities $|q|^2 > Q_0^2$, $Q_0^2 \sim 1 \div 2 \text{ GeV}^2$ being a reasonable cutoff for pQCD being applicable. Pomeron-Pomeron interactions are described by enhanced diagrams [2], using a phenomenological parameterization of multi-Pomeron vertices; essential diagrams are re-summed to all orders. In this approach the contribution of semi-hard processes to the interaction eikonal acquires significant non-factorizable corrections which play an important role for reaching a consistency between the calculated hadronic cross sections and structure functions. On the other hand, such corrections do not appear in corresponding parton momentum distributions and do not contribute to inclusive high- p_t jet spectra.

*e-mail: sergei@ik.fzk.de

2 Linear scheme

Using Gribov's Reggeon approach [1] a high energy hadron-hadron interaction can be described as a multiple scattering process, with elementary re-scatterings being treated phenomenologically as Pomeron exchanges – Fig. 1. The elastic scat-

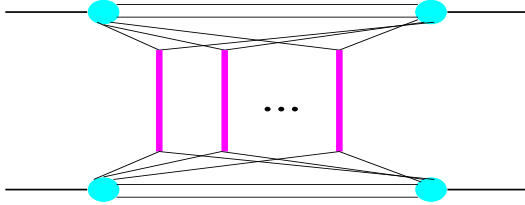


Figure 1: A general multi-Pomeron contribution to hadron-hadron scattering amplitude; elementary scattering processes (vertical thick lines) are described as Pomeron exchanges.

tering amplitude is obtained as a sum of multi-Pomeron exchange contributions¹ [8, 9]:

$$f_{ad}(s, b) = \frac{i}{C_a C_d} \sum_{n=1}^{\infty} \frac{(-1)^{n-1}}{n!} \times \int \prod_{l=1}^n [dx_l^+ dx_l^- C_a C_d G_{ad}^{\mathbb{P}}(x_l^+ x_l^- s, b)] \times N_a^{(n)}(x_1^+, \dots, x_n^+) N_d^{(n)}(x_1^-, \dots, x_n^-) \quad (1)$$

Here s and b are c.m. energy squared and impact parameter for the interaction, $G_{ad}^{\mathbb{P}}(x^+ x^- s, b)$ is the un-integrated Pomeron exchange eikonal (for fixed values of Pomeron light cone momentum shares x^{\pm}), and $N_a^{(n)}(x_1, \dots, x_n)$ is the light cone momentum distribution of constituent partons – Pomeron “ends” (here, quark-antiquark pairs) in hadron a . The product $C_a C_d$ is the shower enhancement coefficient which accounts for low mass diffraction excitations and for inelastic screening effects.

Assuming a factorized form for $N_a^{(n)}$, i.e. $N_a^{(n)}(x_1, \dots, x_n) = \prod_{i=1}^n N_a^{(1)}(x_i)$, one can simplify Eq. (1) and obtain the usual quasi-eikonal expression for the total cross section [8]:

$$\sigma_{ad}^{\text{tot}}(s) = 2 \text{Im} \int d^2 b f_{ad}(s, b) = \frac{2}{C_a C_d} \int d^2 b \left[1 - e^{-C_a C_d \chi_{ad}^{\mathbb{P}}(s, b)} \right] \quad (2)$$

¹In the high energy limit all amplitudes can be considered as pure imaginary.

$$\chi_{ad}^{\mathbb{P}}(s, b) = \int dx^+ dx^- G_{ad}^{\mathbb{P}}(x^+ x^- s, b) \times N_a^{(1)}(x^+) N_d^{(1)}(x^-), \quad (3)$$

where the vertex $N_a^{(1)}(x)$ can be parameterized as $N_a^{(1)}(x) = x^{-\alpha_{\text{part}}}(1-x)^{\alpha_a^{\text{lead}}}$, with the parameters $\alpha_{\text{part}} \simeq 0$, $\alpha_p^{\text{lead}} \simeq 1.5$ expressed via intercepts of secondary Regge trajectories [8, 9].

In this scheme the Pomeron provides an effective description of a microscopic parton cascade, which mediates the interaction between the projectile and the target hadrons. It is convenient to divide the latter into two parts: “soft” cascade of partons of small virtualities $|q|^2 < Q_0^2$, and a perturbative parton evolution at $|q|^2 > Q_0^2$, $Q_0^2 \sim 1 \div 2 \text{ GeV}^2$ being a reasonable scale for pQCD being applicable. Thus, “general Pomeron” consists of two contributions: “soft” Pomeron for pure non-perturbative process (all $|q|^2 < Q_0^2$) and “semi-hard Pomeron” for a cascade which at least partly develops in the high virtuality region (some $|q|^2 > Q_0^2$) [6, 7] – Fig. 2:

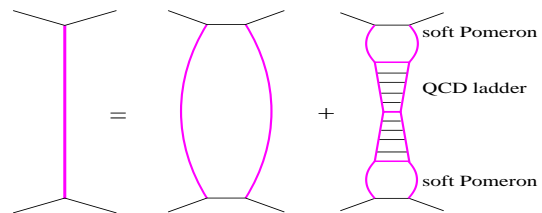


Figure 2: A “general Pomeron” (l.h.s.) consists of the “soft” and the “semi-hard” Pomerons – correspondingly 1st and 2nd graphs in the r.h.s.

$$G_{ad}^{\mathbb{P}}(\hat{s}, b) = G_{ad}^{\mathbb{P}_{\text{soft}}}(\hat{s}, b) + G_{ad}^{\mathbb{P}_{\text{sh}}}(\hat{s}, b) \quad (4)$$

The soft Pomeron eikonal can be chosen as [8]

$$G_{ad}^{\mathbb{P}_{\text{soft}}}(\hat{s}, b) = \frac{\gamma_a \gamma_d (\hat{s}/s_0)^{\alpha_{\mathbb{P}}(0)-1}}{\lambda_{ad}(\hat{s})} e^{-\frac{b^2}{4\lambda_{ad}(\hat{s})}} \quad (5)$$

$$\lambda_{ad}(\hat{s}) = R_a^2 + R_d^2 + \alpha'_{\mathbb{P}}(0) \ln(\hat{s}/s_0), \quad (6)$$

where $s_0 \simeq 1 \text{ GeV}^2$ is the hadronic mass scale, $\alpha_{\mathbb{P}}(0)$ and $\alpha'_{\mathbb{P}}(0)$ are the intercept and the slope of the Pomeron Regge trajectory, and γ_a , R_a^2 are the coupling and the slope of Pomeron-hadron a interaction vertex.

The dominant contribution to the semi-hard Pomeron comes from hard scattering of gluons and sea quarks² and can be represented by a

²For brevity, the contribution of hard scattering of valence quarks is not discussed explicitly.

piece of QCD ladder sandwiched between two soft Pomerons,³ with the eikonal [6, 7]

$$G_{ad}^{\mathbb{P}_{\text{sh}}}(\hat{s}, b) = \frac{1}{2} \sum_{I, J = q(\bar{q}), g} \int d^2 b' \int \frac{dx_h^+}{x_h^+} \frac{dx_h^-}{x_h^-} \times G_{aI}^{\mathbb{P}_{\text{soft}}}(s_0/x_h^+, b') G_{dJ}^{\mathbb{P}_{\text{soft}}}(s_0/x_h^-, |\vec{b} - \vec{b}'|) \times \sigma_{IJ}^{\text{QCD}}(x_h^+ x_h^- \hat{s}, Q_0^2), \quad (7)$$

where $\sigma_{IJ}^{\text{QCD}}(x_h^+ x_h^- \hat{s}, Q_0^2)$ is the contribution of the parton ladder with the virtuality cutoff $|q|^2 > Q_0^2$, I, J and x_h^+, x_h^- are the types and the relative light cone momentum shares of the ladder leg partons. The eikonal $G_{aI}^{\mathbb{P}_{\text{soft}}}(\hat{s}, b')$, describing parton I momentum and impact parameter distribution in the soft Pomeron at virtuality scale Q_0^2 , is defined by Eqs. (5–6), neglecting the small slope of Pomeron-parton coupling $R_I^2 \sim 1/Q_0^2$ and replacing the vertex γ_d by a parameterized Pomeron-parton I vertex $\gamma_I(x_h)$, $x_h = s_0/\hat{s}$ [7, 9]. Convoluting $G_{aI}^{\mathbb{P}_{\text{soft}}}$ with the constituent parton distribution $N_a^{(1)}$ one obtains momentum and impact parameter distribution of parton I in hadron a at virtuality scale Q_0^2 :

$$x f_{I/a}(x, b', Q_0^2) = \int_x^1 dx' N_a^{(1)}(x') \times G_{aI}^{\mathbb{P}_{\text{soft}}}(s_0 x'/x, b') \quad (8)$$

Thus, the contribution of semi-hard processes to the integrated eikonal $\chi_{ad}^{\mathbb{P}}$ (Eq. (3)) can be written as a convolution of hadronic PDFs $f_{I/a(J/d)}(x, b', Q^2)$ (obtained by evolving the input PDFs, Eq. (8), from Q_0^2 to Q^2) with parton scatter cross section $d\sigma_{IJ}^{\text{2J}}/dp_t^2$ [7]:

$$\chi_{ad}^{\mathbb{P}_{\text{sh}}}(s, b) = \frac{1}{2} \int dx^+ dx^- \int dp_t^2 \left\{ K \int d^2 b' \times \sum_{I, J} f_{I/a}(x^+, b', M_F^2) f_{J/d}(x^-, |\vec{b} - \vec{b}'|, M_F^2) \times \frac{d\sigma_{IJ}^{\text{2J}}(x^+ x^- s, p_t^2)}{dp_t^2} \Theta(M_F^2 - Q_0^2) \right\}, \quad (9)$$

with p_t being the parton transverse momentum in the hard process, M_F^2 – the factorization scale (here $M_F^2 = p_t^2/4$), and with the factor $K \simeq 1.5$ accounting for higher order corrections. Integrating the expression in the curly brackets in the r.h.s. of Eq. (9) over \vec{b} one obtains inclusive jet production cross section.

³Similar approaches have been proposed in [10, 11]. In general, one may consider an arbitrary number of t -channel iterations of soft and hard Pomerons [11].

3 Enhanced diagrams

The above-described picture appears to be incomplete in the “dense” regime, i.e. in the limit of high energies and small impact parameters of the interaction. There, a large number of elementary scattering processes occurs and corresponding underlying parton cascades largely overlap and interact with each other [3]. Such effects are traditionally described by enhanced Pomeron diagrams [2]. Assuming that Pomeron-Pomeron interactions are dominated by partonic processes at comparatively low virtualities, $|q^2| < Q_0^2$, multi-Pomeron vertices involve only interactions between soft Pomerons or between “soft ends” of semi-hard Pomerons – Fig. 3. Using an eikonal

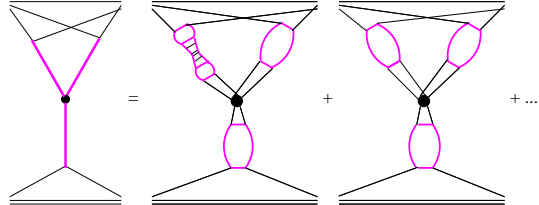


Figure 3: Contributions to the triple-Pomeron vertex from interactions between soft and semi-hard Pomerons.

form for the vertices g_{mn} for the transition of m into n Pomerons, $g_{mn} = r_{3\mathbb{P}} \gamma_{\mathbb{P}}^{m+n-3}$, $r_{3\mathbb{P}}$ being the triple-Pomeron coupling, one can obtain the lowest order contribution, with only one multi-Pomeron vertex, summing over $m, n \geq 1$ and subtracting the term with $m = n = 1$ (Pomeron self-coupling) [12]:

$$\Delta \chi_{ad}^{\mathbb{P}\mathbb{P}(1)}(s, b) = \frac{r_{3\mathbb{P}}}{\gamma_{\mathbb{P}}^3} C_a C_d \int_{\frac{s_0}{s}}^1 \frac{dx_{\mathbb{P}}}{x_{\mathbb{P}}} \int d^2 b' \times \left\{ \left(1 - e^{-C_a \chi_{a\mathbb{P}}^{\mathbb{P}}(s_0/x_{\mathbb{P}}, b')} \right) \times \left(1 - e^{-C_d \chi_{d\mathbb{P}}^{\mathbb{P}}(x_{\mathbb{P}} s, |\vec{b} - \vec{b}'|)} \right) - C_a C_d \chi_{a\mathbb{P}}^{\mathbb{P}}(s_0/x_{\mathbb{P}}, b') \chi_{d\mathbb{P}}^{\mathbb{P}}(x_{\mathbb{P}} s, |\vec{b} - \vec{b}'|) \right\} \quad (10)$$

Here we neglect momentum spread of Pomeron “ends” in multi-Pomeron vertices and define the eikonal $\chi_{a\mathbb{P}}^{\mathbb{P}}$ as

$$\chi_{a\mathbb{P}}^{\mathbb{P}}(\hat{s}, b') = \int_{\frac{s_0}{s}}^1 dx N_a^{(1)}(x) G_{a\mathbb{P}}^{\mathbb{P}}(x \hat{s}, b'), \quad (11)$$

with $G_{a\mathbb{P}}^{\mathbb{P}}(\hat{s}, b')$ given by Eqs. (4–7) under the replacement $\gamma_d \rightarrow \gamma_{\mathbb{P}}$, $R_d^2 \rightarrow R_{\mathbb{P}}^2$, where the

slope of multi-Pomeron vertices is assumed to be small, $R_{\mathbb{P}}^2 \simeq 0$. Correspondingly, for a Pomeron exchanged between two vertices we use $G_{\mathbb{P}\mathbb{P}}^{\mathbb{P}}(\hat{s}, b')$, defined by the same equations under the replacement $\gamma_{a(d)} \rightarrow \gamma_{\mathbb{P}}$, $R_{a(d)}^2 \rightarrow R_{\mathbb{P}}^2 \simeq 0$.

To re-sum higher order contributions it is convenient to start with ones of “fan” type, defined by the recursive equation of Fig. 4:

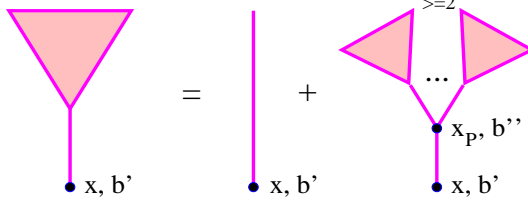


Figure 4: Recursive equation for a “fan” diagram contribution $\chi_a^{\text{fan}}(\hat{s}, b')$, $\hat{s} = s_0/x$.

$$\begin{aligned} \chi_a^{\text{fan}}(\hat{s}, b') &= \chi_{a\mathbb{P}}^{\mathbb{P}}(\hat{s}, b') + \frac{r_{3\mathbb{P}}}{\gamma_{\mathbb{P}}^3 C_a} \\ &\times \int_{\frac{s_0}{\hat{s}}}^1 \frac{dx_{\mathbb{P}}}{x_{\mathbb{P}}} \int d^2 b'' \left[1 - e^{-C_a \chi_a^{\text{fan}}(s_0/x_{\mathbb{P}}, b'')} \right. \\ &\left. - C_a \chi_a^{\text{fan}}(s_0/x_{\mathbb{P}}, b'') \right] G_{\mathbb{P}\mathbb{P}}^{\mathbb{P}}(x_{\mathbb{P}}\hat{s}, |\vec{b}' - \vec{b}''|) \quad (12) \end{aligned}$$

Furthermore, including vertices with both “fans” connected to the projectile and ones connected to the target, one may introduce a “generalized fan” contribution χ_{ad}^{gen} via a recursive equation of Fig. 5:

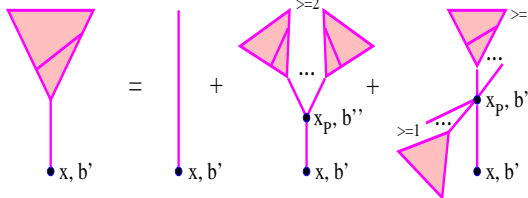


Figure 5: Recursive equation for a “generalized fan” $\chi_{ad}^{\text{gen}}(\hat{s}, \vec{b}', s, \vec{b})$, $\hat{s} = s_0/x$.

$$\begin{aligned} \chi_{ad}^{\text{gen}}(\hat{s}, \vec{b}', s, \vec{b}) &= \chi_{a\mathbb{P}}^{\mathbb{P}}(\hat{s}, b') + \frac{r_{3\mathbb{P}}}{\gamma_{\mathbb{P}}^3 C_a} \\ &\times \int_{\frac{s_0}{\hat{s}}}^1 \frac{dx_{\mathbb{P}}}{x_{\mathbb{P}}} \int d^2 b'' \left\{ \left[1 - e^{-C_a \chi_{ad}^{\text{gen}}(\frac{s_0}{x_{\mathbb{P}}}, \vec{b}'', s, \vec{b})} \right] \right. \\ &\quad \times \exp(-C_d \chi_d^{\text{fan}}(x_{\mathbb{P}}s, |\vec{b} - \vec{b}''|)) \\ &\left. - C_a \chi_{ad}^{\text{gen}}\left(\frac{s_0}{x_{\mathbb{P}}}, \vec{b}'', s, \vec{b}\right) \right\} G_{\mathbb{P}\mathbb{P}}^{\mathbb{P}}(x_{\mathbb{P}}\hat{s}, |\vec{b}' - \vec{b}''|) \quad (13) \end{aligned}$$

For convenience we shall use the symbol of Fig. 6 for the difference between the “generalized fan” and “fan” diagrams.

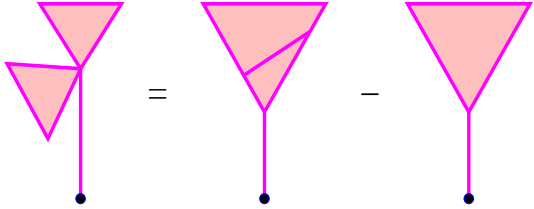


Figure 6: Symbol for the difference between the “generalized fan” and “fan” contributions.

Now, neglecting sub-dominant contributions of Pomeron “loops” and of “chess-board” graphs [5] and re-summing other diagrams to all orders, one gets for hadron-hadron eikonal (Fig. 7)

$$\begin{aligned} \chi_{ad}^{\text{tot}}(s, b) &= \chi_{ad}^{\mathbb{P}}(s, b) + \frac{r_{3\mathbb{P}}}{\gamma_{\mathbb{P}}^3 C_a C_d} \int_{\frac{s_0}{s}}^1 \frac{dx_{\mathbb{P}}}{x_{\mathbb{P}}} \\ &\times \int d^2 b' \left\{ \left(1 - e^{-C_a \chi_{ad}^{\text{gen}}} \right) \left(1 - e^{-C_d \chi_{da}^{\text{gen}}} \right) \right. \\ &\quad - C_a C_d \chi_{ad}^{\text{gen}} \chi_{da}^{\text{gen}} - \left[\frac{C_d}{2} (\chi_{da}^{\text{gen}} - \chi_d^{\text{fan}}) \right. \\ &\quad \times \left(\left(1 - e^{-C_a \chi_{ad}^{\text{gen}}} \right) e^{-C_d \chi_d^{\text{fan}}} - C_a \chi_{ad}^{\text{gen}} \right) \\ &\quad \left. + \frac{C_d}{2} \left(1 - e^{-C_a \chi_a^{\text{fan}}} - C_a \chi_a^{\text{fan}} \right) \right. \\ &\quad \left. \times (\chi_{da}^{\text{gen}} - \chi_{d\mathbb{P}}^{\mathbb{P}}) \right] - [a \leftrightarrow d] \}, \quad (14) \end{aligned}$$

where $\chi_a^{\text{fan}} = \chi_a^{\text{fan}}(\frac{s_0}{x_{\mathbb{P}}}, b')$, $\chi_{a\mathbb{P}}^{\mathbb{P}} = \chi_{a\mathbb{P}}^{\mathbb{P}}(\frac{s_0}{x_{\mathbb{P}}}, b')$, $\chi_d^{\text{fan}} = \chi_d^{\text{fan}}(x_{\mathbb{P}}s, |\vec{b} - \vec{b}'|)$, $\chi_{d\mathbb{P}}^{\mathbb{P}} = \chi_{d\mathbb{P}}^{\mathbb{P}}(x_{\mathbb{P}}s, |\vec{b} - \vec{b}'|)$, $\chi_{ad}^{\text{gen}} = \chi_{ad}^{\text{gen}}(\frac{s_0}{x_{\mathbb{P}}}, \vec{b}', s, \vec{b})$, $\chi_{da}^{\text{gen}} = \chi_{da}^{\text{gen}}(x_{\mathbb{P}}s, \vec{b} - \vec{b}', s, \vec{b})$. The first term in the r.h.s. in Fig. 7 is a simple Pomeron exchange; the second graph contains a multi-Pomeron vertex which couples together any number of “generalized fans” connected to the projectile hadron and any number of those connected to the target; the third graph subtracts Pomeron self-coupling contribution; the other terms in the r.h.s. in Fig. 7 correct for double counts of the same diagrams in the second graph, as can be verified using Figs. 4–6.

4 Results and discussion

Replacing the eikonal $\chi_{ad}^{\mathbb{P}}$ in Eq. (2) by χ_{ad}^{tot} one can calculate total hadron-hadron cross sections, with non-linear screening corrections taken into

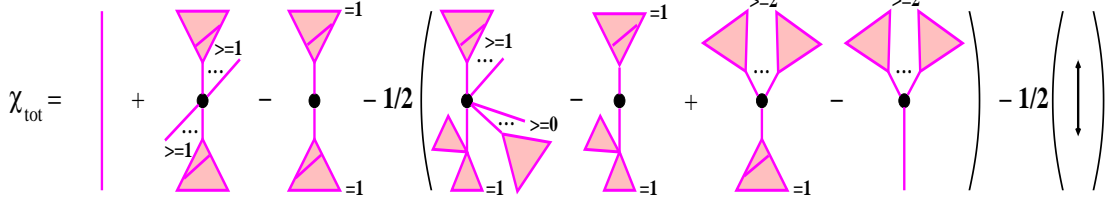


Figure 7: Total hadron-hadron eikonal, including enhanced diagram contributions.

account. On the other hand, one may obtain also gluon and sea (anti-)quark PDFs at the scale Q_0^2 , which acquire non-linear contributions only from “fan” type diagrams of Fig. 4, with the down-most vertex being replaced by the Pomeron-parton coupling. This amounts to replace the eikonal $G_{aI}^{\mathbb{P}}$ ($G_{\mathbb{P}\mathbb{P}}^{\mathbb{P}}$) in Eq. (12) by $G_{aI}^{\mathbb{P}_{\text{soft}}}$ ($G_{\mathbb{P}I}^{\mathbb{P}_{\text{soft}}}$), corresponding to the soft Pomeron exchange⁴ between the parton I and hadron a (nearest multi-Pomeron vertex):

$$x f_{I/a}^{\text{tot}}(x, b', Q_0^2) = x f_{I/a}(x, b', Q_0^2) + \frac{r_{3\mathbb{P}}}{\gamma_{\mathbb{P}}^3 C_a} \times \frac{1}{x_{\mathbb{P}}} \int dx_{\mathbb{P}} \int d^2 b'' \left[1 - e^{-C_a \chi_a^{\text{fan}}\left(\frac{s_0}{x_{\mathbb{P}}}, b''\right)} - C_a \chi_a^{\text{fan}}\left(\frac{s_0}{x_{\mathbb{P}}}, b''\right) \right] G_{\mathbb{P}I}^{\mathbb{P}_{\text{soft}}}\left(\frac{s_0 x_{\mathbb{P}}}{x}, |\vec{b}' - \vec{b}''|\right) \quad (15)$$

Considering unitarity cuts of “fan” diagrams of Fig. 4 corresponding to rapidity gap events, one can calculate also diffractive PDFs [5].

Finally, the parameters of the scheme have been fixed on the basis of experimental data on proton-proton cross section, elastic scattering slope, and on the low x behavior of total and diffractive structure functions; we used $Q_0^2 = 1 \text{ GeV}^2$, $C_p^2 = 1.5$, $\alpha_{\mathbb{P}}(0) = 1.18$, $\alpha'_{\mathbb{P}}(0) = 0.08$, $\gamma_p = 5.6 \text{ GeV}^{-1}$, $R_p^2 = 2.1 \text{ GeV}^{-2}$, $\gamma_{\mathbb{P}} = 1.2 \text{ GeV}^{-1}$, $r_{3\mathbb{P}} = 0.033 \text{ GeV}^{-1.5}$. Fig. 8 shows $\sigma_{pp}^{\text{tot}}(s)$ calculated both with and without enhanced diagram contributions – according to Eq. (2) with the eikonals χ_{ad}^{tot} and $\chi_{ad}^{\mathbb{P}}$ correspondingly. Proton SF $F_2(x, Q^2)$, again calculated with and without enhanced contributions, is shown in Fig. 9. The latter is given to leading order as $F_2(x, Q^2) = \sum_{I=q,\bar{q}} e_I^2 x f_{I/p}(x, Q^2) + F_2^{(c)}(x, Q^2)$, where the

⁴Here semi-hard Pomeron gives a small contribution.

⁵Similar results can be obtained for other choices of Q_0^2 , C_p^2 , $\gamma_{\mathbb{P}}$ (e.g., $Q_0^2=2 \text{ GeV}^2$) [5]; the adjustable parameters are $\alpha_{\mathbb{P}}(0)$, $\alpha'_{\mathbb{P}}(0)$, γ_p , R_p^2 , $r_{3\mathbb{P}}$. Present value of C_p^2 is what one typically obtains from comparison with low mass diffraction pp data [8, 12].

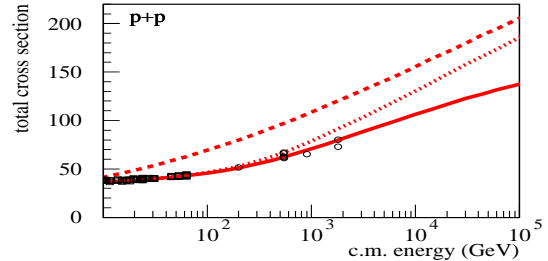


Figure 8: Total pp cross section calculated with and without enhanced diagram contributions, or including only factorizable corrections for the contribution of semi-hard processes – smooth, dashed, and dotted curves correspondingly. The compilation of data is from [13].

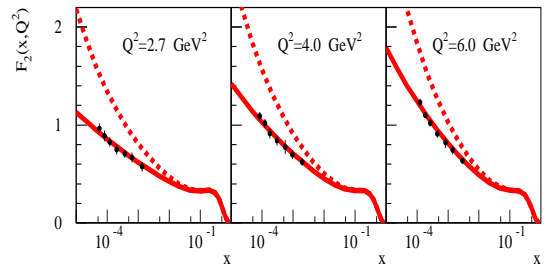


Figure 9: Proton SF F_2 calculated with and without enhanced graph corrections – full and dashed curves. The data are from [14].

(anti-)quark PDFs $f_{q(\bar{q})/p}(x, Q^2)$ are obtained evolving the input ones from the scale Q_0^2 to Q^2 . Here the input sea quark and gluon distributions $f_{q(g)/p}(x, Q_0^2)$ are defined by Eqs. (15) and (8) correspondingly, integrated over \vec{b}' ; for valence quark PDFs $f_{q_v/p}(x, Q^2)$ a parameterized input (GRV94 [15]) has been used. The charm quark contribution $F_2^{(c)}(x, Q^2)$ has been calculated via the photon-gluon fusion process [16].

In a similar way one can calculate diffractive structure function $F_2^{D(3)}(x, x_{\mathbb{P}}, Q^2)$ in the low $\beta = x/x_{\mathbb{P}}$ limit [5], shown in Fig. 10; here $x_{\mathbb{P}}$ defines the rapidity gap size via $y_{\text{gap}} = -\ln x_{\mathbb{P}}$.

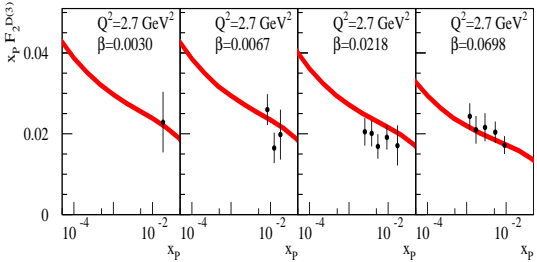


Figure 10: Calculated proton diffractive SF $F_2^D(3)$ compared to ZEUS data [14].

It is important to note that the contribution of semi-hard processes to the eikonal (14) can no longer be expressed in the usual factorized form, Eq. (9). Significant non-factorizable corrections come from graphs where at least one Pomeron is exchanged in parallel to the parton hard process, with the simplest example given by the 1st diagram in the r.h.s. in Fig. 3. In fact, such contributions play an important role for reaching a consistency between calculated total cross sections and structure functions. For illustration, in Fig. 8 shown also the result for $\sigma_{pp}^{\text{tot}}(s)$ obtained with only factorizable corrections taken into account for the semi-hard contribution, i.e. using the eikonal $\bar{\chi}_{pp}(s, b) = \chi_{pp}^{\text{tot(soft)}}(s, b) + \chi_{pp}^{\text{sh(fact)}}(s, b)$. Here the ‘‘soft’’ part $\chi_{pp}^{\text{tot(soft)}}$ is obtained using Eq. (14) and neglecting semi-hard processes (setting $G_{XY}^{\mathbb{P}}(s, b) = G_{XY}^{\mathbb{P}_{\text{soft}}}(s, b)$) in Eqs. (3,11-13), $XY = pp, p\mathbb{P}, \mathbb{P}\mathbb{P}$); the semi-hard eikonal $\chi_{pp}^{\text{sh(fact)}}$ is defined by Eq. (9) with $f_{I/p}(x, b', Q^2)$ obtained from the input distributions $f_{I/p}^{\text{tot}}(x, b', Q_0^2)$, Eq. (15). At the same moment, due to the AGK cancellations [17] the above-mentioned non-factorizable graphs give zero contribution to inclusive high- p_t jet spectra. The latter are always defined in the usual factorized form – by the integrand of Eq. (9), integrated over \vec{b} , and with the PDFs $f_{I/p}(x, b', Q^2)$ containing ‘‘fan’’ diagram screening corrections of Eq. (15).

In conclusion, accounting for non-linear screening effects allows one to obtain a consistent description of total proton-proton cross section and of proton SF F_2 . Although the contribution of semi-hard processes to the interaction eikonal contains an essential non-factorizable part, such non-factorizable diagrams do not contribute to inclusive parton jet spectra and the scheme preserves the QCD factorization picture.

References

- [1] V. N. Gribov, Sov. Phys. JETP **26** (1968) 414; **29** (1969) 483.
- [2] O. Kancheli, JETP Lett. **18** (1973) 274; J. L. Cardi, Nucl. Phys. **B75** (1974) 413.
- [3] L. Gribov, E. Levin, and M. Ryskin, Phys. Rep. **100** (1983) 1.
- [4] L. Durand and P. Hong, Phys. Rev. Lett. **58** (1987) 303; H. N. Wang, Phys. Rep. **280** (1997) 287.
- [5] S. Ostapchenko, Nucl. Phys. Proc. Suppl. (2005), to be published, hep-ph/0412332; hep-ph/0501093.
- [6] N. N. Kalmykov, S. S. Ostapchenko, and A. I. Pavlov, Bull. Russ. Acad. Sci. Phys. **58** (1994) 1966; Nucl. Phys. Proc. Suppl. **52B** (1997) 17.
- [7] H. J. Drescher *et al.*, J. Phys. G: Nucl. Part. Phys. **25** (1999) L91; S. Ostapchenko *et al.*, J. Phys. G: Nucl. Part. Phys. **28** (2002) 2597.
- [8] A. B. Kaidalov and K. A. Ter-Martirosyan, Sov. J. Nucl. Phys. **39** (1984) 979.
- [9] H. J. Drescher *et al.*, Phys. Rep. **350** (2001) 93.
- [10] A. Donnachie and P. Landshoff, Phys. Lett. **B332** (1994) 433.
- [11] S. Bondarenko, E. Levin, and C. I. Tan, Nucl. Phys. **A732** (2004) 73.
- [12] A. B. Kaidalov, L. A. Ponomarev, and K. A. Ter-Martirosyan, Sov. J. Nucl. Phys. **44** (1986) 468.
- [13] C. Caso *et al.*, Eur. Phys. J. C3 (1998) 1.
- [14] S. Chekanov *et al.*, ZEUS Collaboration, Nucl. Phys. **B713** (2005) 3.
- [15] M. Gluck, E. Reya, and A. Vogt, Z. Phys. **C67** (1995) 433.
- [16] M. Gluck, E. Reya, and M. Stratmann, Nucl. Phys. **B422** (1994) 37.
- [17] V. A. Abramovskii, V. N. Gribov, and O. Kancheli, Sov. J. Nucl. Phys. **18** (1974) 308.